 CMES, vol.118, no.3, pp.649-678, 2019

Aerodynamic Characteristics Calculation and Diffusion Law Analysis of Rectangular-Chaff Clouds Under Airflow

Biao Wang[1, *], Yongjian Yang[1] and Hesong Huang[1]

Abstract: To calculate the diffusion law of chaff cloud launched by aircraft, taking rectangular chaff as an example, the diffusion model of chaff cloud is established in this paper. Firstly, the coordinate systems of chaff are defined and the motion model of chaff is established. The motion model mainly includes chaff motion equation and rotation equation, which are obtained by combining the aerodynamic moment and aerodynamic damping. Then, the influence of multi-chaff aerodynamic interference on the movement of chaff is analyzed. Finally, considering the influence of overlap area between chaffs and chaff spacing on the aerodynamic coefficients, the multi-chaff motion model is obtained, and the simulation results are compared with the test results to verify the credibility of the model.

Keywords: Chaff cloud, surface-type infrared decoy, diffusion law, computational fluid dynamics.

1 Introduction

Surface-type infrared decoy is a new form of jamming equipment to counter imaging IR guidance missiles. It is composed of a launcher and thousands of chaffs coated with pyrophoric substance. After launched, thousands of chaffs start diffusing under the force of air flow and gravity, meanwhile, the pyrophoric substance start burning to generate large quantities of heat. This kind of decoy can jam the approaching missiles by forming a similar shape and IR characteristic to its carrier through diffusion and combustion [Lv (2015); SAAB Technologies (2017)]. The research on the diffusion characteristics of chaff cloud formed after the launch of surface-type infrared decoy can not only guide the design of the decoy, but also play an important role in the formulation of its use strategy.

Viau proposed to study the radiation characteristics of airborne surface-type infrared decoy by Monte-Carlo method. Koch also carried out corresponding research work [Viau, D'Agostino and Cathala (2014); Koch and Dochnahl (2000); Koch (2006); Koch (2009)]. Yang Studied on the aerodynamics parameters, and presented a calculation method for parameters based on aerodynamics [Yang (2015); Yang, Chen and Yang (2012)]. Pinchot et al. presented a Chaff cloud Radar Cross Section (RCS) model, able to characterize battle ship autoprotection systems under operational configurations [Pouliguen, Bechu and Pinchot (2005); Pinchot, Béchu and Pouliguen (2017)]. Marcus calculated the RCS of the chaff cloud [Marcus (2004); Marcus (2006); Marcus (2007)]. Pandey presented a modeling

[1] Aeronautics Engineering College, Air Force Engineering University, Xi'an, 710038, China.

[*] Corresponding Author: Biao Wang. Email: kbdbtgyd@sina.com.

and simulation method of chaff cloud using fullwave electromagnetic solver [Pandey (2014)]. Bendayan and Garcia presented a simple assumptions based model that can supply the main spectral characteristics of naval chaff [Bendayan and Garcia (2015)]. Qin and Wu established the compatibility judgment model of SAM and chaff centroid jamming based on the working principle of the two weapons [Qin and Wu (2017)]. Sun et al. introduced a software platform which can simulate and study the countermeasure between the terminal guidance missile and the warship [Sun, Cai, Tang et al. (2011)]. Macedo provided an insight to the application of fuzzy theory to evaluate chaff cloud RCS [Macedo (1997)]. However, most of the models are specific to a particular situation and lack generality, and generally do not consider the aerodynamic damping and aerodynamic interference between chaffs.

Taking rectangular chaff as an example, the diffusion model of chaff cloud is established in this paper. Firstly, the coordinate systems of chaff are defined and the motion model of chaff is established. The motion model mainly includes chaff motion equation and rotation equation, which are obtained by combining the aerodynamic moment and aerodynamic damping. Then, the influence of multi-chaff aerodynamic interference on the movement law of the chaff is analyzed. Finally, considering the overlap area between chaffs and the influence of the chaff spacing on the aerodynamic coefficients, the multi-chaff motion model is obtained, and the simulation results are compared with the test results to verify the credibility of the model.

2 Chaff motion model

As the chaffs are dispersed from each other, and the combustion temperature of the chaff is not high, so the combustion of the foil basically has no influence on its aerodynamic coefficient and diffusion characteristics. In this paper, when calculating the diffusion characteristics of the chaff, the influence of combustion on diffusion is ignored.

2.1 Kinematic equation

Firstly, track coordinate system $Ox_h y_h z_h$, ground coordinate system $Ox_g y_g z_g$, velocity coordinate system $Ox_a y_a z_a$ and body coordinate system $Ox_b y_b z_b$ of chaff are established. The ground coordinate system is an inertial coordinate system fixed on the ground, and its origin is the projection of the launching point on the horizontal plane at the time of chaff launch. The axes Ox_g and Oz_g constitute right-handed rectangular coordinate system with Oy_g in the horizontal plane. The origin of the track coordinate system is the position of the launching point at the time of chaff launch. Ox_h points to the direction of chaff velocity; Oy_h is perpendicular to Ox_h in the lead vertical plane passing through Ox_h. Oz_h, Ox_h and Oy_h constitute the right-handed coordinate system. The origin of the velocity coordinate system is the same as the track coordinate system, and the axis Ox_a coincides with Ox_h. Oy_a is in the plane formed by Ox_a and the chaff axis line, and points upward. Oz_a, Ox_a and Oy_a constitute the right-handed coordinate system. The origin of the body coordinate system is the same as the track coordinate system. Ox_b is parallel

to the short side *a* of the rectangular chaff, and Oz_b is parallel to the long side *b* of the rectangular chaff. Oy_b coincides with the axis line of the chaff nd.

The angle between Ox_h and the horizontal plane is defined as the track pitch angle θ. The angle between Ox_h projection on the horizontal plane and $Ox_g y_g$ is defined as the heading angle ψ_s. The angle between Oy_a and Oy_h is defined as the velocity roll angle γ_s, and when the velocity coordinate system is tilted to the right around Ox_h, γ_s is positive. The diffusion and movement of chaff are calculated in the ground coordinate system. The dynamic equation of chaff is calculated in the track coordinate system.

Because the chaff does not move dynamically, it is only affected by the aerodynamic force and gravity during diffusion. Considering the symmetry and flatness of rectangular chaff, the lateral force can be ignored. The plane composed of chaff axis line and velocity direction is defined as the airflow symmetry plane, then the aerodynamic resistance X and lift force Y of chaff are in the symmetry plane. The dynamic equation of chaff in the track coordinate system is:

$$\begin{cases} m\dfrac{\mathrm{d}V}{\mathrm{d}t} = -X - mg\sin\theta \\ mV\dfrac{\mathrm{d}\theta}{\mathrm{d}t} = Y\cos\gamma_s - mg\cos\theta \\ mV\cos\theta\dfrac{\mathrm{d}\psi_s}{\mathrm{d}t} = -Y\sin\gamma_s \\ X = \dfrac{1}{2}c_x\rho V^2 S \\ Y = \dfrac{1}{2}c_y\rho V^2 S \end{cases} \tag{1}$$

Where, V is chaff speed, θ is chaff track pitch angle, γ_s is speed roll angle, ψ_s is heading angle, c_x、c_y are aerodynamic coefficients, and ρ is atmospheric density.

The angle between the direction of chaff velocity and plane $Ox_b y_b$ in the body coordinate system is defined as the sideslip angle ϖ. Because the length of the long side and the short side of the rectangular chaff are different, the lift coefficient and resistance coefficient in all directions are related not only to the attack angle but also to the sideslip angle. If the unit vectors passing through the center of the chaff and parallel to the short side and the long side of the chaff respectively are $\overrightarrow{nl}$ and $\overrightarrow{nh}$, $\overrightarrow{nd}$ is the unit vector of the chaff axis line, and $\overrightarrow{nh}$ is the outer normal vector of the plane $Ox_b y_b$, then the sideslip angle ϖ is:

$$\varpi = \arcsin\left(\frac{nh_x nv_x + nh_y nv_y + nh_z nv_z}{\sqrt{nh_x^2 + nh_y^2 + nh_z^2}}\right) \tag{2}$$

Where, $\overrightarrow{nv}$ is the unit vector of chaff velocity, nv_x, nv_y and nv_z are its components on three axes of the ground coordinate system. Similarly, nd_x, nd_y, nd_z, nl_x, nl_y, nl_z, nh_x, nh_y and nh_z are the components on three axes of the ground coordinate system of $\overrightarrow{nd}$, $\overrightarrow{nl}$ and $\overrightarrow{nh}$ respectively.

If the chaff pitch angle is ϑ, track angle is ψ, and roll angle is γ, then:

$$\begin{cases} nl_x = \cos\psi\cos\vartheta \\ nl_y = \sin\vartheta \\ nl_z = -\sin\psi\cos\vartheta \end{cases} \tag{3}$$

Let L_b^g be the transformation matrix from the body coordinate system to the ground coordinate system, then $\overrightarrow{nd}$ and $\overrightarrow{nh}$ can be calculated:

$$\begin{bmatrix} nd_x \\ nd_y \\ nd_z \end{bmatrix} = L_b^g \begin{bmatrix} 0 \\ 1 \\ 0 \end{bmatrix} = \begin{bmatrix} -\sin\vartheta\cos\psi\cos\gamma + \sin\psi\sin\gamma \\ \cos\vartheta\cos\gamma \\ \sin\vartheta\sin\psi\cos\gamma + \cos\psi\sin\gamma \end{bmatrix} \tag{4}$$

$$\begin{bmatrix} nh_x \\ nh_y \\ nh_z \end{bmatrix} = L_b^g \begin{bmatrix} 0 \\ 0 \\ 1 \end{bmatrix} = \begin{bmatrix} \sin\vartheta\cos\psi\sin\gamma + \sin\psi\cos\gamma \\ -\cos\vartheta\sin\gamma \\ -\sin\vartheta\sin\psi\sin\gamma + \cos\psi\cos\gamma \end{bmatrix} \tag{5}$$

Considering the aerodynamic interference between chaff movements, the aerodynamic coefficients of chaff are:

$$\begin{cases} c_x = a_x' c_x' \\ c_y = a_y' c_y' \end{cases} \tag{6}$$

Where, c_x' and c_y' are respectively the resistance coefficient and lift coefficient of chaff when there is no aerodynamic interference; a_x' and a_y' are the influencing factors of aerodynamic interference. The solution method will be introduced in the Section 3.

The kinematics equation of the chaff is

$$\begin{cases} \dfrac{\mathrm{d}x_\mathrm{g}}{\mathrm{d}t} = V\cos\theta\cos\psi_\mathrm{s} \\ \dfrac{\mathrm{d}y_\mathrm{g}}{\mathrm{d}t} = V\sin\theta \\ \dfrac{\mathrm{d}z_\mathrm{g}}{\mathrm{d}t} = -V\cos\theta\sin\psi_\mathrm{s} \end{cases} \tag{7}$$

Where, x_g, y_g and z_g are the coordinates of chaff in the ground coordinate system. The components of chaff velocity unit vector on the three axes in the ground coordinate system

are:

$$\begin{cases} nv_x = \cos\theta\cos\psi_s \\ nv_y = \sin\theta \\ nv_z = -\cos\theta\sin\psi_s \end{cases} \tag{8}$$

Let $\overrightarrow{ny}$ be the unit vector of aerodynamic lift , ny_x , ny_y and ny_z be its components on three axes:

$$\overrightarrow{ny} = \frac{\overrightarrow{nv}\times(\overrightarrow{nv}\times\overrightarrow{nd})(\overrightarrow{nv}\bullet\overrightarrow{nd})}{\left|\overrightarrow{nv}\times(\overrightarrow{nv}\times\overrightarrow{nd})(\overrightarrow{nv}\bullet\overrightarrow{nd})\right|} \tag{9}$$

Then, the angle of attack α and speed roll angle γ_s can be expressed as:

$$\gamma_s = -\arcsin\frac{(nv_z ny_x - nv_x ny_z)ny_y}{\sqrt{nv_x^2 + nv_z^2}\left|ny_y\right|} \tag{10}$$

$$\alpha = \frac{\left|\pi/2 - \left|\arccos(\overrightarrow{nd}\bullet\overrightarrow{nv})\right|\right| ny_y}{\left|ny_y\right|} \tag{11}$$

2.2 Chaff rotation model

The rotation of rectangular chaff is much more complicated than that of circular chaff. In the process of rotation, the angular velocity vector of rectangular chaff may not be in the plane $Ox_b y_b$, so the aerodynamic damping moment generated by rotation of chaff is different from the direction of the angular velocity vector, which leads to the constant change of the direction of the angular velocity vector of rectangular chaff.

In the process of chaff movement, the moment is mainly generated by lift force. The moment equation is expressed in the body coordinate system as:

$$J\dot{\overrightarrow{\omega_b}} = \overrightarrow{x_F}\times\overrightarrow{Y_b} - \overrightarrow{M_d} \tag{12}$$

Where, $\overrightarrow{Y_b}$ is the lift force of chaff in the body coordinate system, J is the moment of inertia, $\overrightarrow{\omega_b}$ is the rotation angular velocity in the body coordinate system, $\overrightarrow{M_d}$ is the aerodynamic damping moment, and $\overrightarrow{x_F}$ is the vector from the chaff center to the pressure center. First, the moment of inertia is calculated.

If the rotation angular velocity vector of chaff is $\overrightarrow{\omega_b}$, and the angles between $\overrightarrow{\omega_b}$ and $\overrightarrow{nl}$, $\overrightarrow{nh}$, $\overrightarrow{nd}$ are β , ε , Ω , respectively, as shown in Fig. 1, the relationship between them can be known as:

$$\begin{cases} \cos\Omega = \omega_y / |\omega| \\ \cos\varepsilon = \omega_z / |\omega| \\ \cos\beta = \omega_x / |\omega| \end{cases} \tag{13}$$

Where, $|\omega|$ is the magnitude of $\overrightarrow{\omega_b}$, ω_x, ω_y and ω_z are respectively the components of $\overrightarrow{\omega_b}$ on axis Ox_b, Oy_b and Oz_b.

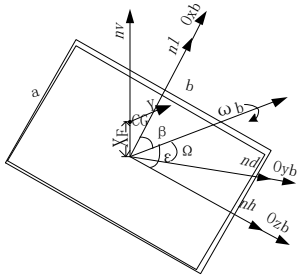

Figure 1: Chaff torque diagram

Let I_{xx}, I_{yy}, I_{zz} be the inertia moments of chaff in axis Ox_b, Oy_b and Oz_b respectively, and their values are [Leylek, Ward and Costello (2012)]:

$$\begin{cases} I_{xx} = mb^2/12 \\ I_{yy} = m\left(a^2 + b^2\right)/12 \\ I_{zz} = ma^2/12 \end{cases} \tag{14}$$

Then, the moment of inertia of the chaff around $\overrightarrow{\omega_b}$ can be obtained as:

$$\begin{aligned} J &= \left[\cos\beta \cos\Omega \cos\varepsilon\right] \begin{bmatrix} I_{xx} & 0 & 0 \\ 0 & I_{yy} & 0 \\ 0 & 0 & I_{zz} \end{bmatrix} \begin{bmatrix} \cos\beta \\ \cos\Omega \\ \cos\varepsilon \end{bmatrix} \\ &= I_{xx}\cos^2\beta + I_{yy}\cos^2\Omega + I_{zz}\cos^2\varepsilon \\ &= \frac{m[b^2(\cos^2\beta + \cos^2\Omega) + a^2(\cos^2\varepsilon + \cos^2\Omega)]}{12} \end{aligned} \tag{15}$$

Let $\overrightarrow{ny_b}$ be the value of the aerodynamic lift unit vector $\overrightarrow{ny}$ in the body coordinate system, and its value is:

$$\overrightarrow{ny_b}^T = L_g^b \overrightarrow{ny}^T \tag{16}$$

Then $\overrightarrow{Y_b}$ is:

$$\vec{Y}_b = |Y|\overrightarrow{ny_b} \tag{17}$$

2.3 Influence of aerodynamic damping on chaff rotation speed

Since the angle between the angular velocity vector $\overrightarrow{\omega_b}$ and the chaff plane is very small, $\overrightarrow{\omega_b}$ is projected into the plane Ox_bz_b to get $\overrightarrow{\omega_b'}$, so the aerodynamic damping moment $\overrightarrow{M_d}$ can be considered as generated by the chaff rotating around $\overrightarrow{\omega_b'}$, as shown in Fig. 2.

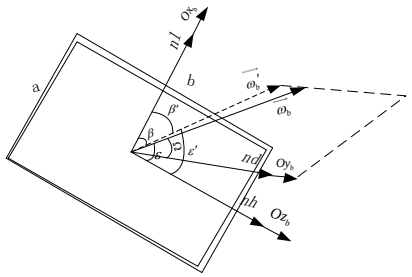

Figure 2: The angular relationship between chaff rotation velocity and body coordinate system

According to the geometric relationship between $\overrightarrow{\omega_b}$ and $\overrightarrow{\omega_b'}$, the angles between $\overrightarrow{\omega_b'}$ and Ox_b , Oz_b are:

$$\begin{cases} \beta' = \text{-arccos}(\cos\beta/|\sin\Omega|)\,\omega_z/|\omega_z| \\ \varepsilon' = \arccos\left(|\cos\varepsilon/\sin\Omega|\right) \\ |\omega_b'| = |\omega||\sin\Omega| \end{cases} \tag{18}$$

Take the microelement ds parallel to $\overrightarrow{\omega_b'}$, as shown in Fig. 3, then the resistance due to rotation is:

$$\mathrm{d}F_d = \frac{1}{2}c_x^{2/\pi}\rho(\omega_b' r)^2\,\mathrm{d}s \tag{19}$$

Where, $c_x^{2/\pi}$ is the resistance coefficient when the angle of attack is $\frac{2}{\pi}$, r is the distance from ds to $\overrightarrow{\omega_b'}$. Then, the aerodynamic damping moment of chaff is:

$$\begin{aligned} M_{dx} &= -c_x^{2/\pi}\rho\omega_b'^2\left(\int_0^{r_1} r^3\frac{a}{\sin^2\varepsilon'}\mathrm{d}r + \int_{r_1}^{r_2} r^2\left(\frac{r_2-r}{\cos\varepsilon'\sin\varepsilon'}\right)\left(\frac{r_1+r}{2\sin\varepsilon'}\right)dr\right)\omega_x/|\omega_x| \\ &= -\frac{c_x^{2/\pi}\rho\omega_b'^2\omega_x}{120\sin^2\varepsilon'\cos\varepsilon'|\omega_x|}\left(30ar_1^4\cos\varepsilon' + 5r_1r_2^4 - 35r_2r_1^4 + 3r_2^5 + 27r_1^5\right) \end{aligned} \tag{20}$$

$$\begin{aligned} M_{dz} &= -c_x^{2/\pi}\rho\omega_b'^2\left(\int_{r_1}^{r_2} r^2\frac{(r_2-r)^2}{2\cos^2\varepsilon'\sin\varepsilon'}dr\right)\omega_z/|\omega_z| \\ &= -\frac{c_x^{2/\pi}\rho\omega_b'^2\omega_z}{60\cos^2\varepsilon'\sin\varepsilon'|\omega_z|}\left(r_2^5 - 10r_2^2r_1^3 + 15r_2r_1^4 - 6r_1^5\right) \end{aligned} \tag{21}$$

When $\varepsilon' = 90^0$, $M_{dx} = -c_x^{\frac{\pi}{2}} \rho \omega_b'^2 ab^4 \omega_x \Big/ 2^6 |\omega_x|$, $M_{dz} = 0$; when $\varepsilon' = 0^0$, $M_{dz} = -c_x^{\frac{\pi}{2}} \rho \omega_b'^2 ba^4 \omega_z \Big/ 2^6 |\omega_z|$, $M_{dx} = 0$. Because $\overrightarrow{\omega_b'}$ is in the chaff plane, $M_{dy} = 0$. $r_1 = b\sin\varepsilon'/2 - a\cos\varepsilon'/2$, $r_2 = b\sin\varepsilon'/2 + a\cos\varepsilon'/2$; M_{dx} , M_{dy} , M_{dz} are the components of $\overrightarrow{M_d}$ on Ox_b , Oy_b and Oz_b .

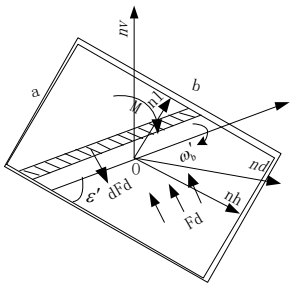

Figure 3: Analysis of chaff rotation moment

The equations of motion and rotation of chaff can be obtained by combining the above formulas.

Take the center of chaff as the origin O ; the direction of $\overrightarrow{\omega_b}$ as the positive direction of Ox_ω ; Oz_ω parallel to the chaff plane, positive to the right; Oy_ω , Ox_ω and Oz_ω constitute the right-handed coordinate system. Then the rotation coordinate system is established. The transformation matrix from the rotation coordinate system to the body coordinate system is:

$$L_\omega^b = \begin{bmatrix} \sin(\Omega)\cos\beta' & -\cos(\Omega)\cos\beta' & \sin\beta' \\ \cos(\Omega) & \sin(\Omega) & 0 \\ -\sin(\Omega)\sin\beta' & \cos(\Omega)\sin\beta' & \cos\beta' \end{bmatrix} \tag{22}$$

$$L_b^\omega = \begin{bmatrix} \sin(\Omega)\cos\beta' & \cos(\Omega) & -\sin(\Omega)\sin\beta' \\ -\cos(\Omega)\cos\beta' & \sin(\Omega) & \cos(\Omega)\sin\beta' \\ \sin\beta' & 0 & \cos\beta' \end{bmatrix} \tag{23}$$

Then, the components of $\overrightarrow{nl}$, $\overrightarrow{nh}$ and $\overrightarrow{nd}$ in the rotational coordinate system can be obtained:

$$\overrightarrow{nl_\omega} = L_b^\omega \begin{bmatrix} 1 \\ 0 \\ 0 \end{bmatrix} = \left(\sin(\Omega)\cos\beta', -\cos(\Omega)\cos\beta', \sin\beta'\right) \tag{24}$$

$$\overrightarrow{nh_\omega} = L_b^\omega \begin{bmatrix} 0 \\ 0 \\ 1 \end{bmatrix} = \left(-\sin(\Omega)\sin\beta', \cos(\Omega)\sin\beta', \cos\beta'\right) \tag{25}$$

$$\overrightarrow{nd_\omega} = L_b^\omega \begin{bmatrix} 0 \\ 1 \\ 0 \end{bmatrix} = \left(\cos(\Omega), \sin(\Omega), 0\right) \tag{26}$$

If $\overrightarrow{nl_\omega}$, $\overrightarrow{nh_\omega}$ and $\overrightarrow{nd_\omega}$ are projected into the $Oy_\omega z_\omega$ plane respectively, the angle between $\overrightarrow{nl_\omega}, \overrightarrow{nh_\omega}, \overrightarrow{nd_\omega}$ and Oy_ω is ∂, χ, υ:

$$\begin{cases} \partial = \left(\dfrac{1}{2} - \dfrac{nl_{\omega y}}{2\left|nl_{\omega y}\right|}\right)\pi + \dfrac{nl_{\omega y}}{\left|nl_{\omega y}\right|}\arcsin\left(\dfrac{nl_{\omega z}}{\sqrt{nl_{\omega y}^2 + nl_{\omega z}^2}}\right) \\ \chi = \left(\dfrac{1}{2} - \dfrac{nh_{\omega y}}{2\left|nh_{\omega y}\right|}\right)\pi + \dfrac{nh_{\omega y}}{\left|nh_{\omega y}\right|}\arcsin\left(\dfrac{nh_{\omega z}}{\sqrt{nh_{\omega y}^2 + nh_{\omega z}^2}}\right) \\ \upsilon = \left(\dfrac{1}{2} - \dfrac{nd_{\omega y}}{2\left|nd_{\omega y}\right|}\right)\pi \end{cases} \tag{27}$$

Then, after time Δt, $\overrightarrow{nd}$, $\overrightarrow{nl}$ and $\overrightarrow{nh}$ are respectively expressed in the rotation coordinate system as:

$$\begin{aligned} \overrightarrow{nl_\omega} = (&nl_{\omega x}, \cos\left(\partial + \omega_b \Delta t\right)\sqrt{nl_{\omega y}^2 + nl_{\omega z}^2} \\ &, \sin\left(\partial + \omega_b \Delta t\right)\sqrt{nl_{\omega y}^2 + nl_{\omega z}^2}) \end{aligned} \tag{28}$$

$$\begin{aligned} \overrightarrow{nh_\omega} = (&nh_{\omega x}, \cos\left(\chi + \omega_b \Delta t\right)\sqrt{nh_{\omega y}^2 + nh_{\omega z}^2} \\ &, \sin\left(\chi + \omega_b \Delta t\right)\sqrt{nh_{\omega y}^2 + nh_{\omega z}^2}) \end{aligned} \tag{29}$$

$$\begin{aligned} \overrightarrow{nd_\omega} = (&nd_{\omega x}, \cos\left(\upsilon + \omega_b \Delta t\right)\sqrt{nd_{\omega y}^2 + nd_{\omega z}^2} \\ &, \sin\left(\upsilon + \omega_b \Delta t\right)\sqrt{nd_{\omega y}^2 + nd_{\omega z}^2}) \end{aligned} \tag{30}$$

So after time Δt, $\overrightarrow{nd}$, $\overrightarrow{nl}$ and $\overrightarrow{nh}$ are:

$$\begin{cases} \overrightarrow{nd}^T = L_b^g L_\omega^b \overrightarrow{nd_\omega}^T \\ \overrightarrow{nl}^T = L_b^g L_\omega^b \overrightarrow{nl_\omega}^T \\ \overrightarrow{nh}^T = L_b^g L_\omega^b \overrightarrow{nh_\omega}^T \end{cases} \tag{31}$$

3 Aerodynamic interference model

In the process of movement, aerodynamic force of chaff is disturbed by other nearby chaff, which has a great influence on c_x and c_y of chaff. In this section, CFD (Computational Fluid Dynamics) is used to calculate the flow field of single chaff without aerodynamic interference and the mutual interference between chaffs, and finally the aerodynamic interference factors a'_x and a'_y are solved

3.1 Aerodynamic coefficients without aerodynamic interference

In this part, aerodynamic coefficients of chaff without aerodynamic interference are calculated. The SST turbulence model, RSM turbulence model and $k-\varepsilon$ turbulence model are respectively applied to calculate aerodynamic coefficients of rectangular chaff without aerodynamic interference. Then, by comparing the calculated results with the wind tunnel test results, the most accurate turbulence model is selected, and the aerodynamic coefficients of chaff at different speeds, angles of attack and side-slip angles are calculated. Finally, the aerodynamic coefficient database of chaff is obtained.

3.1.1 Wind tunnel test

Rectangular chaff wind tunnel test is conducted in low-speed wind tunnel. The wind tunnel test section is 2 m in length, the section shape is square, the inlet and outlet size are both 1.2 m*1.2 m, the wind tunnel flow field quality is good, turbulence $\varepsilon \le 1\%$, the maximum available wind speed is 0.6 Ma. The rectangular chaff with a size of 30*25 mm is installed on a six-component force balance, and its measurement accuracy is 0.1-0.2%. The experimental wind speed is 0.6 Ma, the static pressure at the entrance is 98.56 kPa, the total pressure is 124.37 kPa, the static temperature is 78.1°C. The aerodynamic coefficients of the rectangular chaff are measured respectively for $\varpi = 0^0$ and $\varpi = 90^0$. When $\varpi = 0^0$, the velocity vector of the incoming flow is in the plane Ox_by_b of the body coordinate system. When $\varpi = 90^0$, the velocity vector of the incoming flow is in the plane Oy_bz_b of the body coordinate system. Then the aerodynamic coefficient curves of the rectangular chaff measured by the test are shown as Fig. 4.

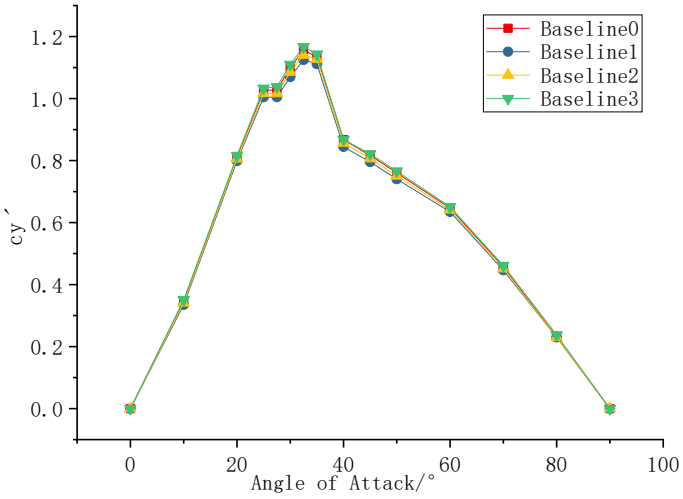

a) lift coefficient

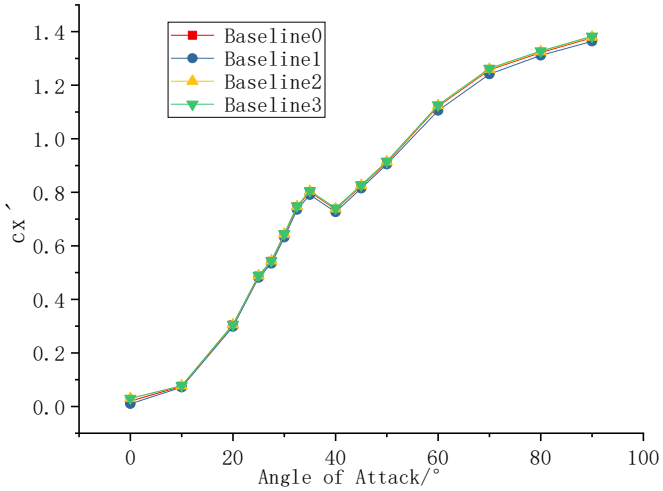

b) drag coefficient

Figure 4: Wind tunnel test results

As can be seen from the figure, the test curve is relatively smooth and there is no obvious jump point. The four measurements showed good coincidence, which indicates that the test result of the six-component force balance is relatively accurate, and the force measurement system has a good stability. The stall attack angle of the chaff is 32.5°, and the maximum lift coefficient is 1.1569.

3.1.2 Comparison of CFD calculation results with wind tunnel tests

PIM-PLE algorithm is used to solve the Navier-Stokes equation. The spatial discretization method based on the finite volume method and the linear interpolation method based on

the second-order spatial accuracy is used, and the second-order precision backward difference method is used for time discretization. The inlet and outlet as well as the outer wall of the calculation domain are set as the pressure far field, and the chaff surface is set as the non-slip wall surface. The RSM turbulence model, SST turbulence model and $K-\varepsilon$ turbulence model are selected as the calculation models, and the results of different turbulence models are compared.

Let the size of chaff be 30*25 mm, and the calculated region be a cuboid of 600*300* 300 mm. In the direction of incoming flow, since the flow field above and in front of the chaff has little influence on the flow field of the calculation domain, in order to improve the calculation accuracy without increasing the number of grids, the chaff is placed at the upper left corner of the calculation domain, as shown in Fig. 5. The center of the chaff is 150 mm from the front surface of the calculation domain and 50 mm from the upper surface of the calculation domain. The thickness of the first layer of boundary layer grid is 10^{-6} m. Hexagonal structure grid is adopted. The total number of grids is 3.977 million, as shown in Fig. 6 and Fig. 7. The initial conditions are altitude $\mathrm{H}=0$, pressure $P=101325\,Pa$, atmospheric temperature $T=288.15\,\mathrm{K}$, inlet Mach number $Ma=0.6$. When the sideslip Angle is $\varpi=90^{0}$, the comparison between the results calculated by different models and the test is shown in Fig. 8.

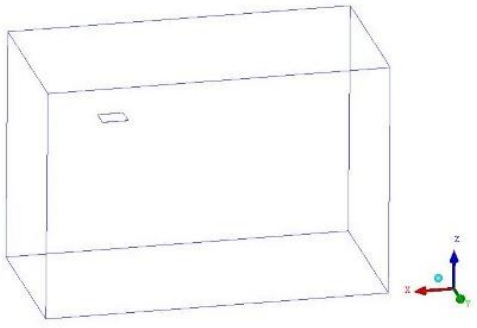

Figure 5: The calculation zone of chaff

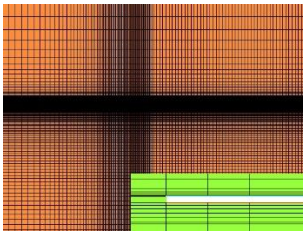

Figure 6: The schematic diagram of hexahedron structure grid and chaff boundary layer grid in the domain

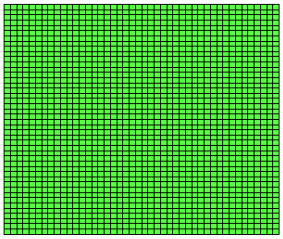

Figure 7: Schematic diagram of rectangular chaff surface mesh

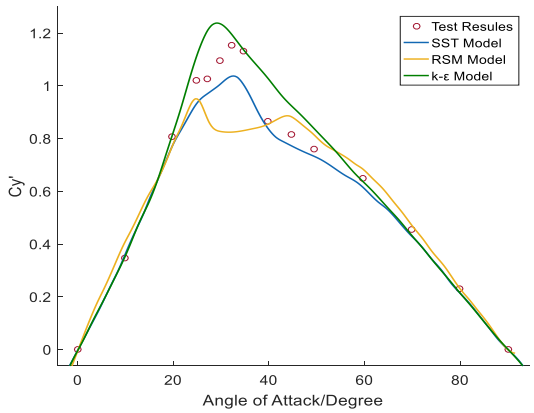

Figure 8: When sideslip Angle $\varpi = 90^0$, the comparison between calculated results at different angles of attack and the test results

It can be seen from the figure that the SST turbulence model is in good agreement with the experimental results for the flow field calculation of rectangular chaff. It can be seen from the comparison between the wind tunnel test results in Tab. 1 and the calculation results of the SST turbulence model that the maximum calculation error of the SST turbulence model is 8.9%, and the results are very accurate. Therefore, the SST turbulence model is selected in this paper to calculate the flow field of rectangular chaff. The aerodynamic coefficients of chaff when the speed of chaff changes within the range of 0.1-1.2Ma are calculated by SST model, and the angle of attack and sideslip vary from 0^0 to 90^0. Moreover, the aerodynamic coefficient database of rectangular chaff without aerodynamic interference is established, so as to obtain the aerodynamic coefficients c_x' and c_y'

Table 1: The relationship between chaff aerodynamic coefficient and angle of attack

Angle of attack	c_x'		c_y'		x_F	
	Num.	Exp.	Num.	Exp.	Num.	Exp.
20^0	0.283	0.304	0.789	0.809	0.00401	0.00415
30^0	0.602	0.641	1.002	1.100	0.00381	0.00379
45^0	0.774	0.823	0.777	0.817	0.00446	0.00462
60^0	1.042	1.121	0.626	0.647	0.00721	0.00749
80^0	1.282	1.322	0.231	0.222	0.01567	0.01703

To illustrate the grid independence in CFD calculation, lift coefficient curves at 0.95 million 2.03 million, 2.81 million, 3.97 million and 5.1 million are calculated respectively.

The calculation conditions are consistent with Fig. 9. SST turbulence model is adopted, and the calculation results are shown in the figure below. As can be seen from the figure, when the number of grids increases from 0.95 million to 3.97 million, the calculation result changes obviously, while when the number increases from 3.97 million to 5.1 million, it changes little. Therefore, it is reasonable to use 3.97 million grids to calculate the aerodynamic coefficient of foil.

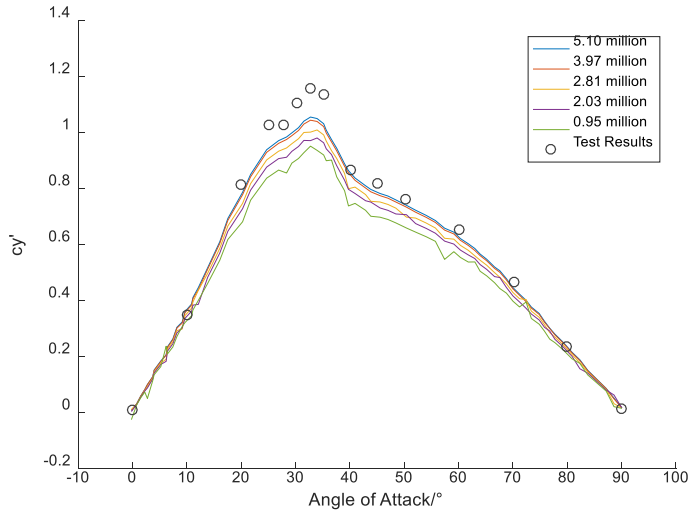

Figure 9: Grid independence validation

The SST turbulence model is applied to calculate the chaff sideslip angle $\varpi = 0^0$ and $\varpi = 90^0$ respectively, and the chaff pressure distribution when the angle of attack varies from 0^0 to 90^0, as shown in the Fig. 10 and Fig. 11.

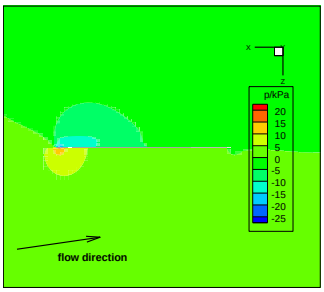

(a) 10^0

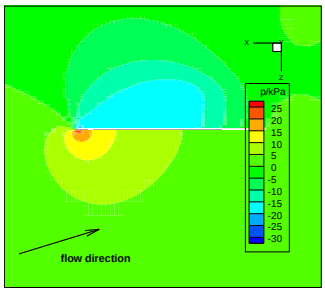

(b) 20^0

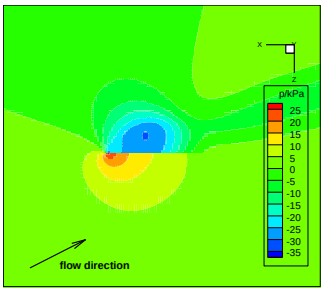

(c) 30^0

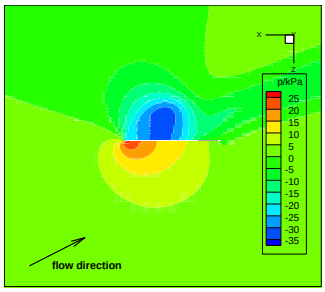

(d) 35^0

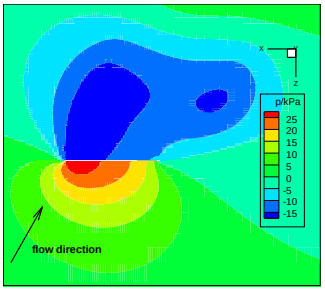

(e) 60^0

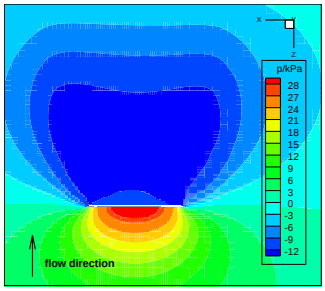

(f) 90^0

Figure 10: Chaff pressure distribution diagram when sideslip angle $\varpi = 90^0$

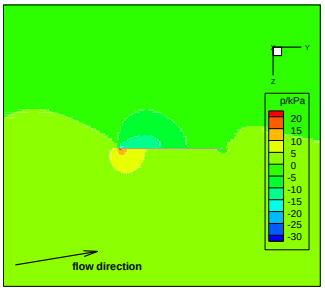

(a) 10^0

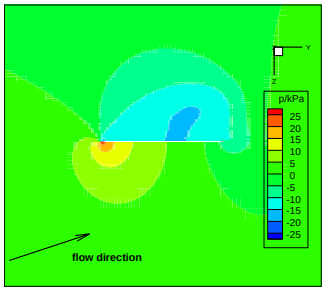

(b) 20^0

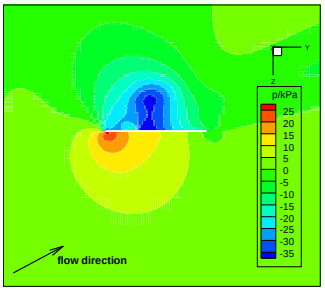

(c) 30^0

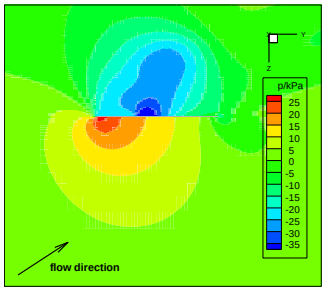

(d) 35^0

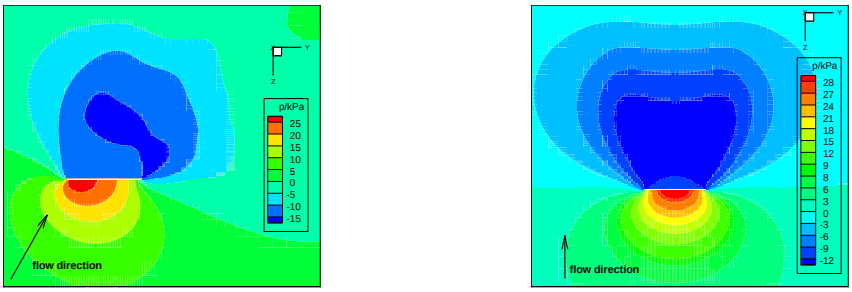

(e) 60^0 (f) 90^0

Figure 11: Chaff pressure distribution diagram when sideslip angle $\varpi = 0^0$

As can be seen from Fig. 10 and Fig. 11, the pressure distribution diagram of chaff with $\varpi = 0^0$ and $\varpi = 90^0$ is relatively similar, indicating that there is little difference in the flow field of rectangular chaff at sideslip $\varpi = 0^0$ and $\varpi = 90^0$. With the increase of the angle of attack, the negative pressure area at the leading edge of the chaff increases gradually, and c_y' also increases gradually. When the angle of attack is greater than 30^0, the negative pressure area at the back edge of the chaff gradually decreases, indicating that the boundary layer near the back edge of the chaff starts to separate due to the influence of strong adverse pressure gradient, and the separation point gradually moves forward with the increase of the attack angle, resulting in a decrease in lift and c_y'. However, the induced resistance of chaff increases with the increase of the attack angle, so that c_x' increases with the increase of the attack angle.

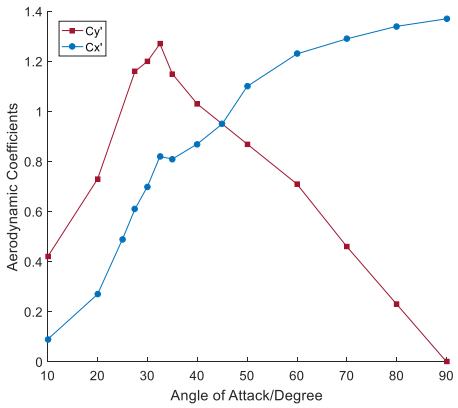

Figure 12: Calculation results of SST turbulence model when $\varpi = 0^0$

Fig. 12 shows the aerodynamic coefficient changing with the angle of attack when the chaff sideslip angle $\varpi = 0^0$. As can be seen from Fig. 8 and Fig. 12, the aerodynamic coefficient of the chaff is slightly larger at $\varpi = 0^0$ than that at $\varpi = 90^0$. Meanwhile, Figs. 11(c) and

11(d) have larger negative pressure region on the surface of chaff than Figs. 10 (c) and 10(d). Therefore, when $\varpi = 0^0$ and the attack angle is α=30^0 or α=35^0, the lift coefficient of the chaff is larger than that at $\varpi = 90^0$, that is, when the sideslip angle $\varpi = 0^0$, the maximum lift coefficient of the chaff is greater than that at the sideslip angle $\varpi = 90^0$. When $\varpi = 0^0$, the aspect ratio of the chaff is slightly larger than that of $\varpi = 90^0$, which results in that at the same angle of attack, the vortex strength of the chaff tip at $\varpi = 0^0$ is smaller than that at $\varpi = 90^0$, and the downwash effect of the chaff is also smaller. Therefore, the effective angle of attack at $\varpi = 0^0$ is larger than that at $\varpi = 90^0$, resulting in that the lift coefficient of the chaff at $\varpi = 0^0$ is greater than that at $\varpi = 90^0$ before stall, and the aerodynamic performance of the chaff is better.

3.2 Influence of aerodynamic interference on aerodynamic coefficient of chaff

According to the CFD flow field calculation in Section 3.1.2, SST turbulence model has high accuracy in calculating the outflow field of rectangular chaff. Therefore, SST turbulence model is also used in this section to calculate the aerodynamic coefficient of chaff when there is aerodynamic interference between them. In the initial stage of diffusion, there are overlaps, occlusions and interference between chaffs, and the distance between the chaffs is relatively close, so aerodynamic interference between the chaff cannot be ignored.

3.2.1 Coincidence area interference

Because the projection shape of rectangular chaff on another chaff is not standard, it is very complicated to calculate the overlap area between rectangular chaffs. In order to simplify the calculation and ensure a certain accuracy, the rectangular chaff is transformed into a circular chaff with the same area, and the overlap area between the transformed circular chaff is calculated. Then the radius *R* of the converted rectangular chaff is:

$$R=\sqrt{\text{a*b}/\pi} \tag{32}$$

The chaff is projected in its movement direction, and the aerodynamic interference caused by other chaffs behind the chaff is ignored, so that an elliptical cylinder region can be obtained in space (Fig. 13 dotted line region). When other chaffs move into this region during the movement, it is considered that there is interference to its aerodynamic characteristics, otherwise there is no interference.

Suppose the central coordinate of chaff j is $\left(x_j, y_j, z_j\right)$, the unit vector of velocity is $\overrightarrow{nv}$, and the unit vector of axis line is $\overrightarrow{nd_j}$. There is a chaff k in its projection region, and the central coordinate is $\left(x_k, y_k, z_k\right)$, the unit vector of velocity is $\overrightarrow{nv_k}$, and the unit vector of axis line is $\overrightarrow{nd_k}$, as shown in Fig. 13, then:

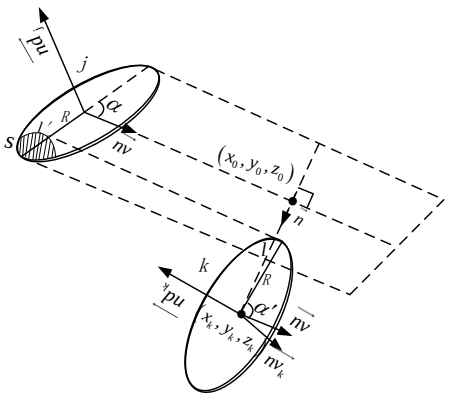

Figure 13: Schematic diagram of chaff overlapping area

l is the overlap length of chaff j in the projection region of chaff k. There is coincidence when $l > 0$ and no coincidence when $l \le 0$. l' is the value obtained by projecting l onto the plane of chaff j, and s is the coincidence area.

Let x_0, y_0, z_0 be the intersection points between the vertical line perpendicular to $\overrightarrow{nv}$ at the center of the circle of chaff k and the central line of projection area of chaff j, then:

$$\begin{cases} d = nv_x x_k + nv_y y_k + nv_z z_k \\ x_0 = \dfrac{\left(nv_z{}^2 x_j - nv_z nv_x z_j + nv_y{}^2 x_j - nv_y nv_x y_j + nv_x d\right)}{nv_x{}^2 + nv_y{}^2 + nv_z{}^2} \\ y_0 = \dfrac{\left(-nv_y nv_z z_j + nv_y d - nv_y x_j nv_x + y_j nv_z{}^2 + nv_x{}^2 y_j\right)}{nv_x{}^2 + nv_y{}^2 + nv_z{}^2} \\ z_0 = \dfrac{\left(-nv_z nv_y y_j + nv_z d - nv_z x_j nv_x + z_j nv_y{}^2 + nv_x{}^2 z_j\right)}{nv_x{}^2 + nv_y{}^2 + nv_z{}^2} \end{cases} \tag{33}$$

Set $\vec{n}$ as the unit vector that (x_0, y_0, z_0) points to (x_k, y_k, z_k), and project the chaff j and the chaff k in the direction of the velocity unit vector $\overrightarrow{nv}$ of the chaff j to the plane perpendicular to $\overrightarrow{nv}$ with the center of the chaff k, then the ellipse j and the ellipse k can be obtained. The radii of ellipse j and k are:

$$\begin{cases} R_j = \sqrt{\left(R\cos\phi_j\right)^2 + \left(\left|\overrightarrow{nd_j}\cdot\overrightarrow{nv}\right|R\sin\phi_j\right)^2} \\ R_k = \sqrt{\left(R\cos\phi_k\right)^2 + \left(\left|\overrightarrow{nd_k}\cdot\overrightarrow{nv}\right|R\sin\phi_k\right)^2} \\ \phi_j = \arccos\left(\dfrac{\left(\overrightarrow{nd_j}\times\overrightarrow{nv}\right)\cdot\vec{n}}{\left|\overrightarrow{nd_j}\times\overrightarrow{nv}\right|}\right) \\ \phi_k = \arccos\left(\dfrac{\left(\overrightarrow{nd_k}\times\overrightarrow{nv}\right)\cdot\vec{n}}{\left|\overrightarrow{nd_k}\times\overrightarrow{nv}\right|}\right) \end{cases} \tag{34}$$

Where, R_j and R_k are respectively the radius of the ellipse j and k in the direction of vector $\vec{n}$, ϕ_j and ϕ_k are respectively the angle between R_j , R_k and the long axis of the ellipse. Then the coincidence length l is:

$$l = R_k - \sqrt{\left(x_0 - x_k\right)^2 + \left(y_0 - y_k\right)^2 + \left(z_0 - z_k\right)^2} + R_j \tag{35}$$

Project l into the plane of chaff j to obtain:

$$l' = lR/R_j \tag{36}$$

If $l'' = l'/2$, then the overlap area s is approximately:

$$s = \begin{cases} 2*[R^2 * \arccos\left(\left(R - l''\right)/R\right) \\ \qquad -\sqrt{2*R*l'' - l''^2} * \left(R - l''\right)]*\lambda & l'' < R \\ \pi * R^2 * \lambda & l'' \geq R \end{cases} \tag{37}$$

Where, λ and $\vec{t}$ are:

$$\lambda = \cos(\arcsin((nd_{xk} * t_x + nd_{yk} * t_y + nd_{zk} * t_z) / \sqrt{t_x^2 + t_y^2 + t_z^2})) \tag{38}$$

$$\vec{t} = \overrightarrow{nv} \times (x_k - x_j, y_k - y_j, z_k - z_j) \tag{39}$$

3.2.2 Distance interference

This section mainly calculates the expression of distance impact factor a_l. If the upper and lower chaffs are parallel to each other, and the sideslip angle, angle of attack and direction of motion are the same, then when the line of the upper and lower chaffs' center is parallel to the direction of motion, the overlap area $s = \pi R^2/2$. As can be seen from Zou et al. [Zou (2016); Huang, Tong, Chai et al. (2018)]:

$$\begin{cases} a'_x = 1 - a_l \\ a'_y = k a'_x \end{cases} \tag{40}$$

Where a'_x and a'_y are aerodynamic interference factors of drag and lift respectively, a_l is the distance interference factor. Assume two chaffs parallel to each other, the angle between the line connecting the center of them and the horizontal plane is 30°, The lower chaff is in front of the upper chaff, and the two chaffs move downward in an oblique direction. The speed of upper and lower chaff is the same, and the direction of them is the same as the line connecting the center of the two chaff, the sideslip angle of two chaffs is 0°, and the angle of attack is 30°, as shown in Fig. 14.

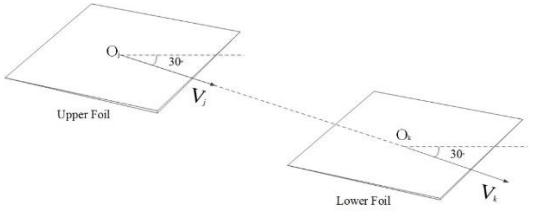

Figure 14: Schematic diagram of chaff position

The SST turbulence model is applied to calculate the aerodynamic coefficients of each chaff when the distance between the center of the upper chaff and the lower chaff is from 0.5R to 10R, as shown in Fig. 15:

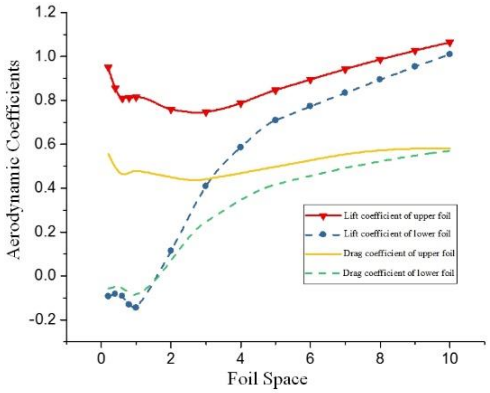

Figure 15: The relationship between chaff aerodynamic coefficient and chaff spacing

Then, the relationship between aerodynamic interference factors a'_x and a'_y with chaff spacing can be obtained, as shown in Fig. 16:

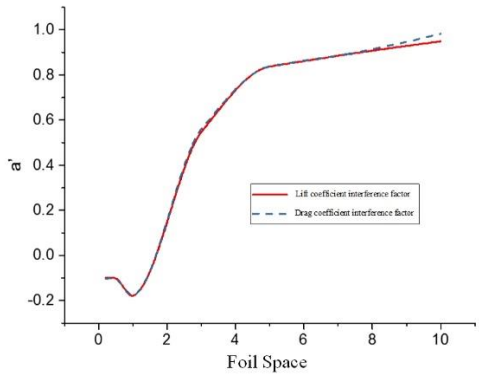

Figure 16: The relationship between aerodynamic interference factors and chaff spacing

According to the results of CFD calculation, the value of a'_x and a'_y is very close, so for rectangular chaff, a'_x is considered to be equal to a'_y, that is, $k=1$.

By fitting the curve of a'_x, the approximate expression of the distance influencing factor a_l can be obtained as follows:

$$a_l=\begin{cases}-1.413*(r/R)^4+2.968*(r/R)^3-1.922*(r/R)^2+0.489*(r/R)+1.056, & r\le R\\ -0.889*(r/R)^2+0.896*(r/R)+0.952, & R<r<10R\\ 0, & r\ge 10R\end{cases} \tag{41}$$

3.2.3 Interference model validation

In this part, CFD is mainly used to verify the aerodynamic interference influencing factors a'_x and a'_y of rectangular chaff. First, aerodynamic interference between parallel chaffs is verified. Suppose the size of rectangular chaff is 30* 25 mm, the upper and lower chaffs are parallel to the horizontal plane, and the distance from the center of them is $R=\sqrt{30*25/\pi}$ mm. The position relationship between the two chaffs is shown in Fig. 17. The two pieces of chaff move downward in an oblique direction with the same speed and sideslip angle of $\varpi=0^0$. Then, the chaff flow field at different angles of attack calculated by CFD is shown as follows:

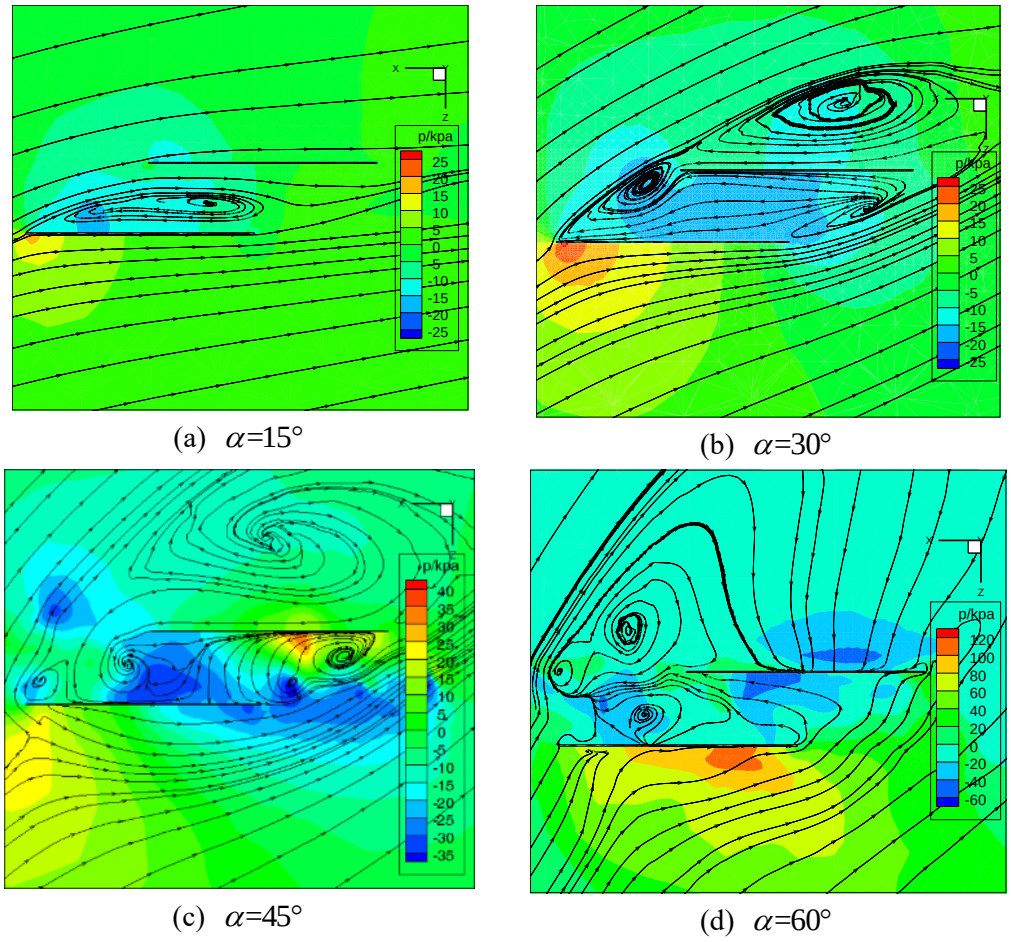

(a) α=15° (b) α=30°

(c) α=45° (d) α=60°

Figure 17: CFD calculation results

Aerodynamic interference is calculated by using formulas (33)-(39), and is compared with CFD calculation results, as shown in Tab. 2.

Table 2: The calculation result comparison of aerodynamic interference factors of parallel chaff

Angle of attack α	a'_x		a'_y	
	CFD results	Calculation results	CFD results	Calculation results
15°	0.231	0.481	0.234	0.481
30°	-0.178	-0.178	-0.176	-0.178
45°	0.051	0.054	0.042	0.054
60°	0.209	0.203	0.195	0.203

Then, aerodynamic interference between non-parallel chaffs is verified. Let the angle between the line connecting the center of the upper and lower two chaffs and the horizontal plane be $30°$, and the two chaffs move downward and in the same direction parallel to the line of the center of them. The angle between the upper chaff and the horizontal plane is ρ. It is defined that the angle between the upper chaff and the horizontal plane is positive when the upper chaff rotates clockwise. The sideslip angle of upper and lower chaff is the same $\varpi = 0^0$. Then the attack angle of the lower chaff is $\alpha = 30°$, and the attack angle of the upper chaff is $\alpha = 30° - \rho$, as shown in Fig. 18. CFD is used to calculate the aerodynamic coefficients and aerodynamic interference influencing factors of upper and lower chaff when the angle is changed. The calculation results are shown in Fig. 19.

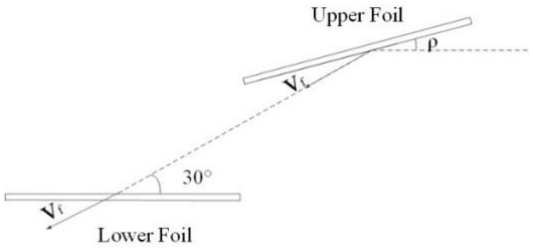

Figure 18: Schematic diagram of chaff position

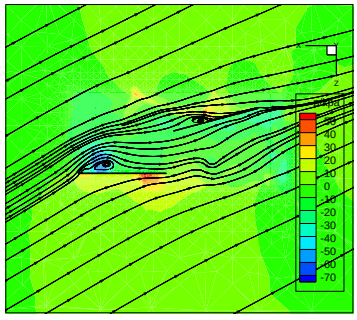

(a) ρ=15°

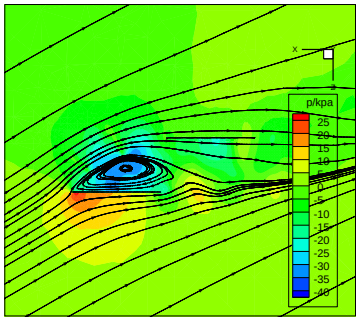

(b) ρ=0°

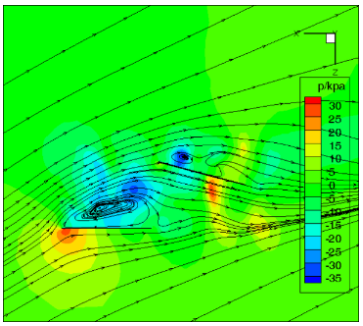

(c) ρ=-15°

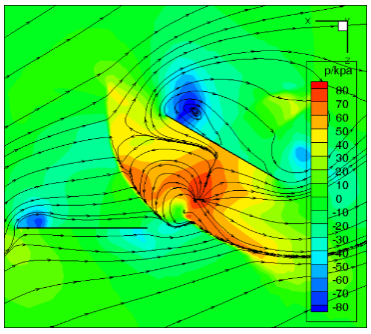

(d) ρ=-30°

Figure 19: CFD calculation results

The aerodynamic interference model of rectangular chaff is used to calculate the aerodynamic interference. And the calculation results are compared with the CFD results. The comparison results are shown in Tab. 3:

Table 3: The calculation result comparison of aerodynamic interference factors of non-parallel chaff

Angle ρ	a'_x		a'_y	
	CFD results	Calculation results	CFD results	Calculation results
15°	0.094	0.149	0.096	0.149
0°	0.104	0.149	0.127	0.149
–15°	0.263	0.281	0.365	0.281
–30°	0.305	0.382	0.309	0.382

As can be seen from the comparison results in Tab. 2 and Tab. 3, the rectangular aerodynamic interference model has little difference from the CFD calculation results and the change trend is the same.

4 Chaff cloud motion model

According to the chaff motion model, aerodynamic interference model, aerodynamic coefficients when the chaff is free of aerodynamic interference calculated by CFD, and the initial information of each chaff, the multi-chaff motion model can be solved. The solution process is mainly based on the position, attitude and flow field of each chaff at the previous moment, to calculate the position and attitude of each chaff in the space at the next moment, and then to obtain the diffusion movement law of multi-chaff cloud at any time.

Due to the influence of random factors such as atmospheric disturbances, the initial attitude of each chaff has some difference. After the comparison and analysis with the measured data, it is approximately believed that the initial pitch angle, yaw angle and roll angle of the chaff all obey the uniform distribution of $U(-\pi/2,\pi/2)$. Then, the initial axial line vectors of different chaff $\overrightarrow{nd}$ can be obtained by formula (4), and the initial $\overrightarrow{nl}$ and $\overrightarrow{nh}$ of each chaff can also be obtained by formula (3) and (5). Since the initial velocity of the chaff is known, the initial track pitch angle and heading angle can be obtained from formula (8).

The specific simulation process of multi-chaff motion model is as follows: if the axis line vector, track pitch angle, heading angle, velocity and coordinate position of *N* chaffs at time *t* are known, the solution process of the *i*th chaff at time *t* is: the aerodynamic interference factor of chaff *i* can be obtained from formula (32), formula (37), formula (40) and formula (41), and its aerodynamic coefficient can be obtained from formula (6). The position coordinate, track pitch angle, heading angle and velocity of chaff *i* at time $t+\Delta t$ can be obtained by substituting them into formula (1) and formula (7). Finally, axis line vectors $\overrightarrow{nd}$, $\overrightarrow{nl}$ and $\overrightarrow{nh}$ of chaff *i* at time $t+\Delta t$ are obtained from formula (22) and formula (28)- formula (31). Then, all the parameters of N chaffs at time $t+\Delta t$ can be

obtained, and finally, the multi-chaff motion model can be solved.

5 Simulation and verification of chaff cloud diffusion

5.1 Chaff cloud diffusion simulation

Let the plane fly horizontally at sea level with a speed of 0.8 Ma. The aircraft is equipped with an infrared decoy launcher which is vertical to the fuselage. The initial launching speed of the chaff is 25 m/s. The velocity direction is perpendicular to the aircraft. The size of the rectangular chaff is 30*25 mm. The simulation results are shown as follows:

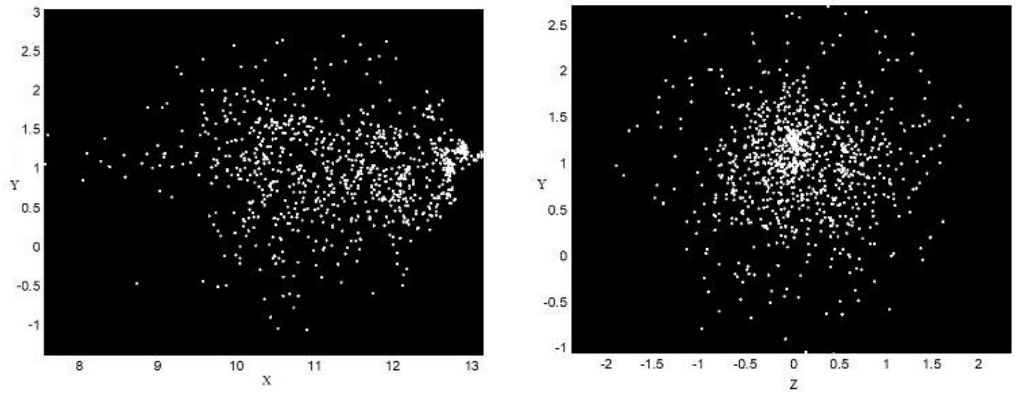

Figure 20: Chaff cloud diffusion image at t=0.05 s

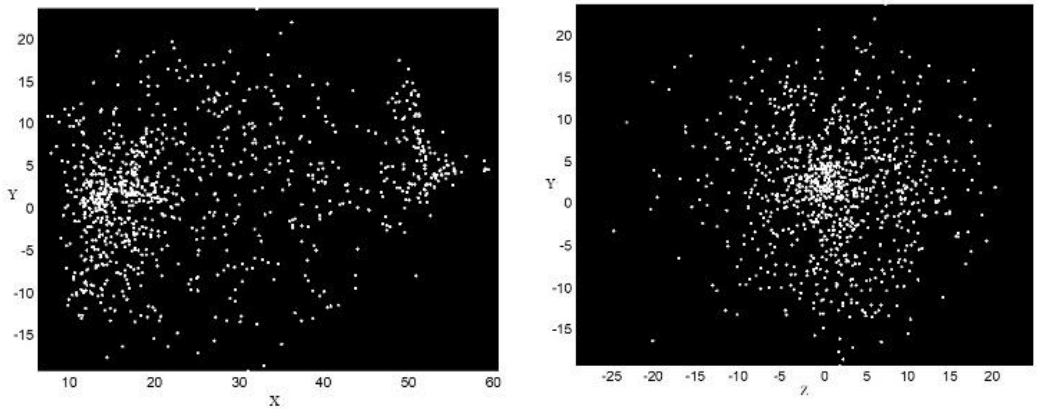

Figure 21: Chaff cloud diffusion image at t=0.5 s

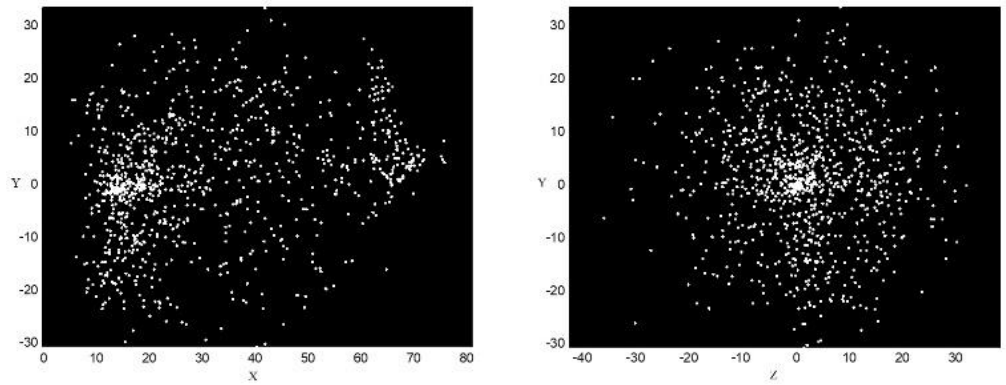

Figure 22: Chaff cloud diffusion image at t=1 s

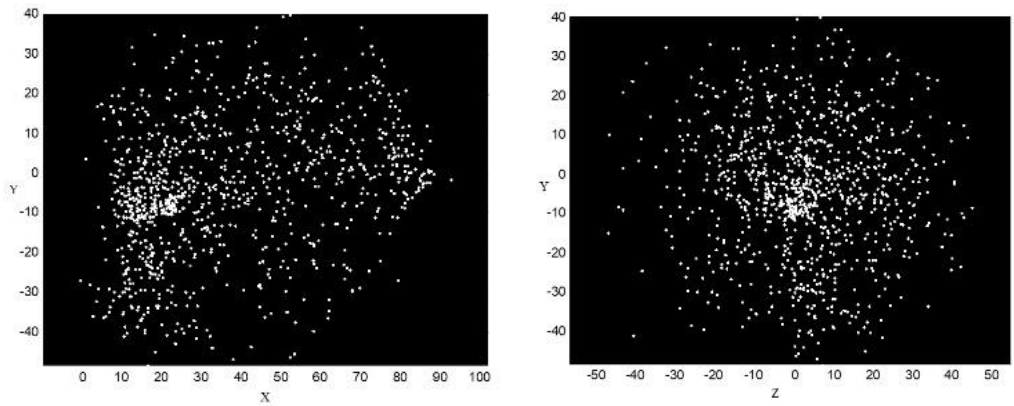

Figure 23: Chaff cloud diffusion image at t=2 s

As can be seen from the simulation results in Fig. 20-Fig. 23, the rectangular chaff cloud mass is roughly conical in distribution with a certain angle to the X-axis. At 0.05 s, the chaff cloud is roughly conical in distribution, with the X-axis diffusion length of 5.5 m and the Z-axis diffusion length of 3.2 m. After 0.5 s, the chaff cloud continues to diffuse, with the X-axis diffusion length reaching 58m and the z-axis diffusion length reaching 37 m. After 1s, the chaff cloud has basically diffused into shape, and begins to enter the subsidence stage. The diffusion velocity in the X-axis and Z-axis decreases significantly. After 2 s, the X-axis diffusion length of the chaff cloud finally reaches 90 m and the Z-axis length reaches 82 m.

During the rotation of rectangular chaff cloud, the aerodynamic damping torque of the two micro-elements symmetric with respect to the rotation angular velocity vector $\overrightarrow{\omega_b}$ is inconsistent, resulting in that $\overrightarrow{\omega_b}$ of the chaff always changes in the rotation process, and $\overrightarrow{\omega_b}$ is not necessarily in the plane of the chaff, so the whole rotation process is relatively complex. The aerodynamic force of chaff varies in space, which makes the cloud diffusion area of chaff larger. However, in the rotation process of circular chaff, due to its special symmetry, its rotation angular velocity vector $\overrightarrow{\omega_b}$ is always parallel to the oz_b-axis in the

body coordinate system, so there is no oz_b-axis force in the body coordinate system, and the aerodynamic force of the chaff only changes in the $ox_b y_b$ plane. Therefore, the diffusion area of circular chaff is smaller than that of rectangular chaff.

5.2 Rocket sled experiments

In this part, the credibility of multi-chaff motion model is verified by comparing the experimental results of rocket skid with simulation results. The experimental conditions of rocket skid and circular chaff are similar. SC7700MW infrared thermal imager is used in the experiment. The size of rectangular chaff is 30*25 mm, and the thickness of chaff is 0.1 mm. 1000 pieces of chaff are horizontally compressed in the launch tube, and the launch velocity is vertically upward with a size of 25 m/s. There is no physical adhesion between chaffs. The chaff is coated with spontaneous combustion active metal. The rocket skid track is 3km long, and it ignites at the far left of the track. Two infrared thermal imagers are placed in the middle of the track, 500 m from the track, as shown in Fig. 24. When the rocket skid enters the field of view of infrared thermal imager and launches decoys, the speed of the rocket skid is about 0.7 Ma. The pairs of experimental results and simulation results are shown in Tab. 4:

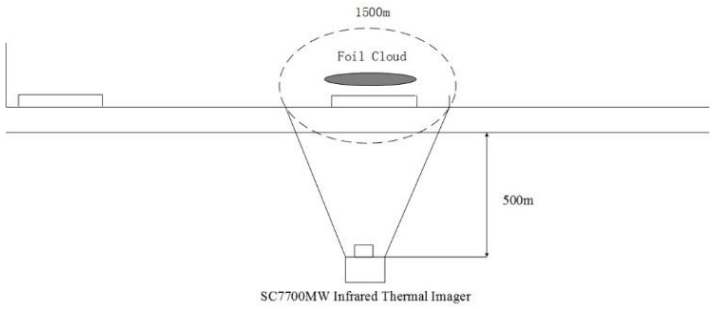

Figure 24: Schematic diagram of rocket sled test

Table 4: Comparison between test and simulation results

	Chaff cloud size/m	Time/s					
		0.2	0.5	0.8	1.0	1.5	2
Test results	X-axis	25.8	55.7	59.6	63.5	71.8	78.5
	Y-axis	17.2	33.4	46.6	52.7	50.9	47.7
	Z-axis	-	-	-	-	-	-
Simulation results	X-axis	27.6	58.4	63.3	68.0	79.4	89.4
	Y-axis	18.2	39.1	53.9	58.9	73.3	81.1
	Z-axis	17.4	37.4	50.7	61.4	70.2	82.6

As can be seen from the diffusion length of chaff cloud measured in the test, rectangular chaff cloud rapidly diffuses under the impact of airflow, with a large diffusion area, and the diffusion length of chaff cloud can reach 78 m. The simulated chaff cloud length is in good agreement with the experimental results within 1s after the interference loading chaff is launched.

After 1 s, the chaff cloud begins to enter the descending stage. Due to the blocking effect of the ground, the diffusion length of the tested chaff cloud on the Y-axis is gradually shortened, while the diffusion length on the X-axis is also slowly increased. According to the simulation results in Fig. 22, nearly half of the chaff has fallen to the ground at 1 s, and the number of chaffs falling to the ground is still increasing. Therefore, after 1 s, the diffusion length of the chaff cloud measured in the experiment on the Y-axis gradually shortens, and the length on the X-axis also grows very slowly, resulting in a large error with the simulation.

Therefore, the rectangular chaff cloud diffusion model established in this section is relatively accurate, with little experimental error, and can reflect the entire movement and diffusion law of chaff cloud.

6 Conclusion

Taking rectangular chaff as an example, the diffusion model of chaff cloud is established in this paper. Through the comparison with wind tunnel test and rocket sled test, it can be seen that the rectangular chaff cloud diffusion model established in this paper is accurate, and can reflect the whole movement and diffusion law of chaff cloud. The main work of this paper is as follows:

(1) A six-dof motion model of a single chaff is established, which takes into account the influence of aerodynamic damping on rotation.

(2) Aerodynamic coefficients of chaffs are calculated and compared with wind tunnel test results, and aerodynamic interference model between chaffs is established.

(3) The whole movement model of chaff cloud is established, and the simulation of the movement of chaff cloud is carried out. The simulation results are compared with the rocket sled test.

Data accessibility

All of the data in this work have been reported in the paper and are freely available.

Funding

This work is supported by the National Natural Science Foundation of China (grant number 61471390).

Declaration of Conflicting Interests

The authors declared no potential conflicts of interest with respect to the research, authorship, and publication of this article.

References

Bendayan, M.; Garcia, A. (2015): Signal modeling of chaff in naval environment

simulation. *IEEE Transactions on Aerospace and Electronic Systems*, vol. 51, no. 4, pp. 3161-3166.

Huang, H.; Tong, Z.; Chai, S.; Zhang, Y. (2018): Experimental and numerical study of chaff cloud kinetic performance under impact of high speed airflow. *Chinese Journal of Aeronautics*, vol. 31, no. 11, pp. 2082-2092.

Koch, E. C.; Dochnahl, A. (2000): IR emission behavior of Magnesium Teflon Viton (MTV) compositions. *Propellants, Explosives, Pyrotechnics*, vol. 25, no. 37, pp. 37-40.

Koch, E. C. (2006): Pyrotechnic countermeasures: II. Advanced aerial infrared countermeasures. *Propellants, Explosives, Pyrotechnics*, vol. 31, no. 1, pp. 3-19.

Koch, E. C. (2009): 2006-2008 annual review on aerial infrared decoy flares. *Propellants Explos Pyrotech*, vol. 34, pp. 6-12

Leylek, E.; Ward, M.; Costello, M. (2012): Flight dynamic simulation for multibody aircraft configurations. *Journal of Guidance Control and Dynamics*, vol. 35, no. 6, pp. 1828-1842.

Lv, M. S. (2015): Approach jamming effectiveness evaluation for surface-type infrared decoy in network centric warship formation. *Optical and Optoelectronic Sensing and Imaging Technology*, pp. 9674.

Macedo, A. D. F. (1997): Analysis of chaff cloud RCS applying fuzzy calculus. *International Microwave & Optoelectronics Conference*.

Marcus, S. W. (2004): Dynamics and radar cross section density of chaff clouds. *IEEE Transactions on Aerospace and Electronic Systems*, vol. 40, no. 1, pp. 93-102.

Marcus, S. W. (2006): The RCS of large dense chaff clouds. *Antennas & Propagation Society International Symposium.*

Marcus, S. W. (2007): Electromagnetic wave propagation through chaff clouds. *IEEE Transactions on Antennas & Propagation*, vol. 55, no. 7, pp. 2032-2042.

Pandey, A. K. (2014): Modeling and simulation of chaff cloud with random orientation and distribution. *International Microwave & Rf Conference.*

Pinchot, J. L.; Béchu, O.; Pouliguen, P. (2017): A chaff cloud modelisation. *International Symposium on Antenna Technology & Applied Electromagnetics*.

Pouliguen, P.; Bechu, O.; Pinchot, J. L. (2005): Simulation of chaff cloud radar cross section. *Antennas & Propagation Society International Symposium*.

Qin, J. D.; Wu, X. F. (2017): Modeling and simulation on the compatibility of ship-to-air missile and chaff centroid jamming in cooperative air-defense. *Advanced Information Technology, Electronic & Automation Control Conference.*

SAAB Technologies (2017): BOL Ensuring Mission Success for F/A-18. https:// saab.com/air/electronic-warfare/countermeasure- dispenser- systems /bol-fa-18/.

Sun, P.; Cai, Q.; Tang, J.; Li, N.; Du, J. (2011): On spreading chaff cloud for countering the terminal guidance missile. *IEEE CIE International Conference on Radar*, pp. 845-849.

Viau, C. R.; D'Agostino, I.; Cathala, T. (2014): Coupling of TESS with SEWORKBENCH for EO/IR countermeasure development and effectiveness assessment. *10th International IR Target and Background Modeling and Simulation Workshop*, pp. 1-14.

Yang, C. L. (2015): Research on infrared decoy radiation characteristics and simulation. *10th Conference on Industrial Electronics and Application*, pp. 1223-1227.

Yang, C. L.; Chen, Y.; Yang, M. D. (2012): Research on infrared decoy movement characteristics and simulation. *7th IEEE Conference on Industrial Electronics and Applications*.